Original Paper

Effect of adsorption-induced matrix swelling on coal permeability evolution of micro-fracture with the real geometry

Ming-Yao Wei [a, b], Jishan Liu [c], Ying-Ke Liu [d, *], Zhang-Hao Liu [e], Derek Elsworth [f]

[a] National and Local Joint Engineering Laboratory of Internet Application Technology on Mine, IoT Perception Mine Research Center, China University of Mining and Technology, Xuzhou 221116, Jiangsu, China
[b] State Key Laboratory of Coal and CBM Co-Mining, Jincheng 048012, Shanxi, China
[c] School of Engineering, The University of Western Australia, 35 Stirling Highway, Perth, WA, 6009, Australia
[d] Faculty of Safety Engineering, China University of Mining and Technology, Xuzhou 221116, Jiangsu, China
[e] Institute of Rock and Soil Mechanics, Chinese Academy of Sciences, Wuhan 430071, Hubei, China
[f] Department of Energy and Mineral Engineering, G3 Center and Energy Institute, The Pennsylvania State University, University Park, PA16802, USA

ARTICLE INFO

ABSTRACT

Gas transport in coal induces effective stress variation, matrix swelling/shrinkage, and significantly affects matrix and fracture deformation, resulting in porosity and permeability evolution. However, the heterogeneity and anisotropy of coal are neglected in dual porosity models, which can lead to the deviation from the real physical mechanisms. To uncover the permeability evolution, especially the influence of dynamic matrix-fracture interaction for real fracture distribution, advanced virtual simulation is proposed. In this study, real fracture geometry is taken into account in the physical model based on the CT-scan image, while the mathematical models for coal deformation and gas flow are established. Our calculations are verified against a long-term experimental data under the same boundary condition. Accordingly, the real matrix-fracture interaction caused by adsorption-induced matrix deformation has been visually exhibited, and some new insight into the behavior of fracture permeability in real materials is offered. The results indicate the non-uniform distribution of fracture geometry is responsible for the nonmonotonic change of permeability. It also found that injection pressure, Langmuir strain constant and initial matrix permeability have important influences on the fracture permeability evolution. This research provides valuable insight into the understanding of the permeability change for the real fracture spatial distribution in coal.

1. Introduction

Coal is generally complex porous medium that composed of pores, fractures (cleats), and matrix solid skeleton, involving discontinuous, heterogeneous, and anisotropic structures. Discontinuous matrix blocks can be treated as solid skeleton which bears external load (Fan and Ettehadtavakkol, 2017). The structure of fracture systems determines the gas seepage characteristics as the major flow paths. Thus, the permeability of fracture is a key characteristic for gas flow behavior in coal reservoir (Connell and Detournay, 2009). Coal deformation can directly affect the

fracture volume variation. During the coal bed methane (CBM) production process, the coal reservoir is influenced by simultaneous changes in effective stress, matrix swelling/shrinkage and pore pressure. The nonuniform fracture distribution induces heterogeneous matrix internal stress distribution. Consequently, matrix deformation is nonuniform, generating non-linear effects on the fracture domain. Due to the small aperture of micro-fractures, coal permeability is particularly sensitive to coal deformation. This makes the coupled gas-solid interaction under in-situ conditions more complex (Liu et al., 2011).

A number of researchers have conducted laboratory works, proposed theoretical models, and performed numerical simulations to investigate the gas-bearing coal deformation and permeability evolution under different confining-pressure or pore-pressure conditions (Connell et al., 2010; Wang et al., 2014; Shi

* Corresponding author.
E-mail addresses: cumtwmy@sina.com (M.-Y. Wei), liuyk-cumt@163.com (Y.-K. Liu).

et al., 2018; Liu et al., 2016). Existing permeability models are mainly developed based on the poroelasticity theory (Seidle and Huitt, 1995; Robertson and Christiansen, 2008; Shi and Durucan, 2005; Palmer and Mansoori, 1996). It is believed that the permeability would increase due to the effective stress reduction from the pore pressure increment under a fixed confining pressure. Thus, there should be a monotone positive correlation between pore pressure and coal permeability. Actually, this relationship tends to be merely suitable for conventional reservoirs with relatively high permeability. Classical permeability models assume an instantaneous matrix-fracture pressure equilibrium state can be achieved with synchronous matrix and fracture deformation (Seidle and Huitt, 1995; Palmer and Mansoori, 1996; Shi and Durucan, 2005; Robertson and Christiansen, 2008; Liu et al., 2011). The instantaneous equilibrium assumption of these models ignores the influence of matrix-fracture interactions on permeability evolution. Besides, the majority of permeability measurements are completed within several days. Matrix pressure deviates significantly from the equilibrium pressure during the experiments because of the low matrix permeability, while researchers always hypothesize matrix pore pressure reaches the equilibrium level shortly after injection and believe the samples are under static equilibrium testing conditions. In reality, the time required to realize the equilibrium state is considerably longer than the testing time scale (Wu et al., 2017) and the pressure equilibrium of the entire system has not been achieved. As a result, the laboratory observations can hardly reflect the influence of the pore-pressure equilibrium process. Since coal micro-fractures dominate gas transport, the gas-solid coupling characteristics are different from the typical steady-state coupling ones and conventional coupling methods show inability in appropriately describing the entire gas flow procedure (Wei et al., 2019a). In order to accurately depict the gas seepage within fracture systems and analyze the coupled relation between seepage and stress fields, modeling of the micro-fracture structure should be addressed.

Numerical simulation is currently regarded as an effective tool to replicate the real gas transport process in coal. Numerical models can be classified into the following two types: equivalent-continuum models and discrete fracture network models. Typical continuum dual-porosity modeling involves averaged characterization of matrix and fracture properties, which cannot accurately characterize the nonuniform spatial distribution of the realistic fracture (Liu et al., 2020). As for discrete fracture network models, they idealize complex fracture networks as interconnected pore space that separates matrix blocks (spherical matrix models, matchstick matrix models, capillary models, and cubic matrix models) (Al-Kharusi and Blunt, 2007). Liu et al. (2020) investigated the impact of non-uniform swelling on the evolution of permeability from initial to ultimate equilibrium with a regular array of the matrix-fracture geometry. However, this approach fails to predict the coal permeability after CH_4 injection. The reason may be attributed to that these idealized fracture structures cannot reflect the actual fracture geometry (He et al., 2015). High-resolution SEM images are also used to calibrate the micro-CT images and measure the exact aperture size of fractures and estimate permeability (Mostaghimi et al., 2017). These studies only focus on the static properties of coal fractures. Wu et al. (2010) built a geometry model of artificial split coal based on CT images. The microscale interaction within the coal fractures is missed in this study. Previous studies fail to capture the micro-fracture distribution and permeability evolution under the influence of non-uniform deformation. To make up for the limitations of the two types of models, this research utilizes fracture geometry obtained from CT scanning images of core samples to reconstruct the actual micro-fracture spatial distribution and establish numerical models for coupled

matrix and fracture gas flow. This allows for better analyses of adsorption-induced matrix and fracture deformation, and quantify the influence of the non-uniform and heterogeneous nature of fracture systems on permeability evolution.

2. Conceptual model

There are two distinct factors that affect coal permeability during pressure depletion in coal reservoir. The first is an increasing effective stress that leads to a decrease in the coal permeability. The second is desorption-induced shrinkage that results in an increase in the coal permeability. These two competitive impacts account for the change in coal permeability (Brochard et al., 2012; Cui et al., 2007; Nikoosokhan et al. 2012, 2014; Shi and Durucan, 2005; Vandamme et al., 2010; Wu et al., 2010). Although many theoretical permeability models have been developed, there are still no clear explanations for the inconsistency of the experimental and model results. Liu et al. (2011) have proposed a concept to understand the interaction between matrix and fracture in the process of gas adsorption. Consider a high permeability fracture surrounded by the matrix as shown in Fig. 1. At the first stage (Stage A), the pressure in the matrix and fracture are initial pressure. If the gas is injected, the gas always fills the fracture space at first due to the high permeability. While the gas pressure in the matrix remains unchanged in stage B. When gas is injected, the swelling deformation principally occurs in the fracture system due to decreasing of effective stress. Because of the pressure difference between fracture and matrix, the gas gradually flows into the matrix. The pressure of region adjacent to fractures increases firstly. The pressure distribution in the matrix is non-uniform in stage C. After gas diffusing into the matrix, adsorption-induced swelling deformation occurs as well as in the matrix system. Matrix swelling is primarily localized in the vicinity of a fracture compartment. Thus, the swelling deformation is larger near the fracture than that far away from the fracture. The competition equilibrium effects within the matrix occurring at the same time lead to diminishing of fracture swell deformation. The space in fracture system reduces in response to the local swelling of the matrix. The gas pressure of matrix is in the non-equilibrium state for a long period compared to fracture. With the gas flow through the matrix, the swelling behavior becomes uniform. As the decreasing of deformation gradient in the matrix, the influence of matrix swelling on the fracture aperture change becomes weak. Because of the homogenizing swelling deformation, the fracture permeability recovers while the effect of local deformation vanishes in stage D.

It could be concluded that the interaction process experiences four stages: (1) initial equilibrium state; (2) fracture permeability enhance induced by increasing of gas pressure; (3) fracture permeability reduction corresponding to the internal shrink squeezed by matrix swelling; and (4) fracture permeability increase corresponding to uniform swelling of the sample.

3. Micro-fracture conceptual model based on CT images

Gas transport within coal block is a complex coupled multiphysics process which involves matrix and fracture deformation, gas flow, and sorption-induced swelling. Previous laboratory studies have investigated the long-term permeability evolution law with gas adsorption (Wei et al., 2019b). However, the matrix-fracture interaction caused by sorption-induced matrix deformation has not been visually exhibited experimentally. To uncover matrix-fracture interaction mechanisms, we reconstruct the fracture structure of the core sample, simulate the CO_2 (adsorbing gas) injection procedure, and analyze the evolution laws of different physical processes during the adsorption equilibrium process.
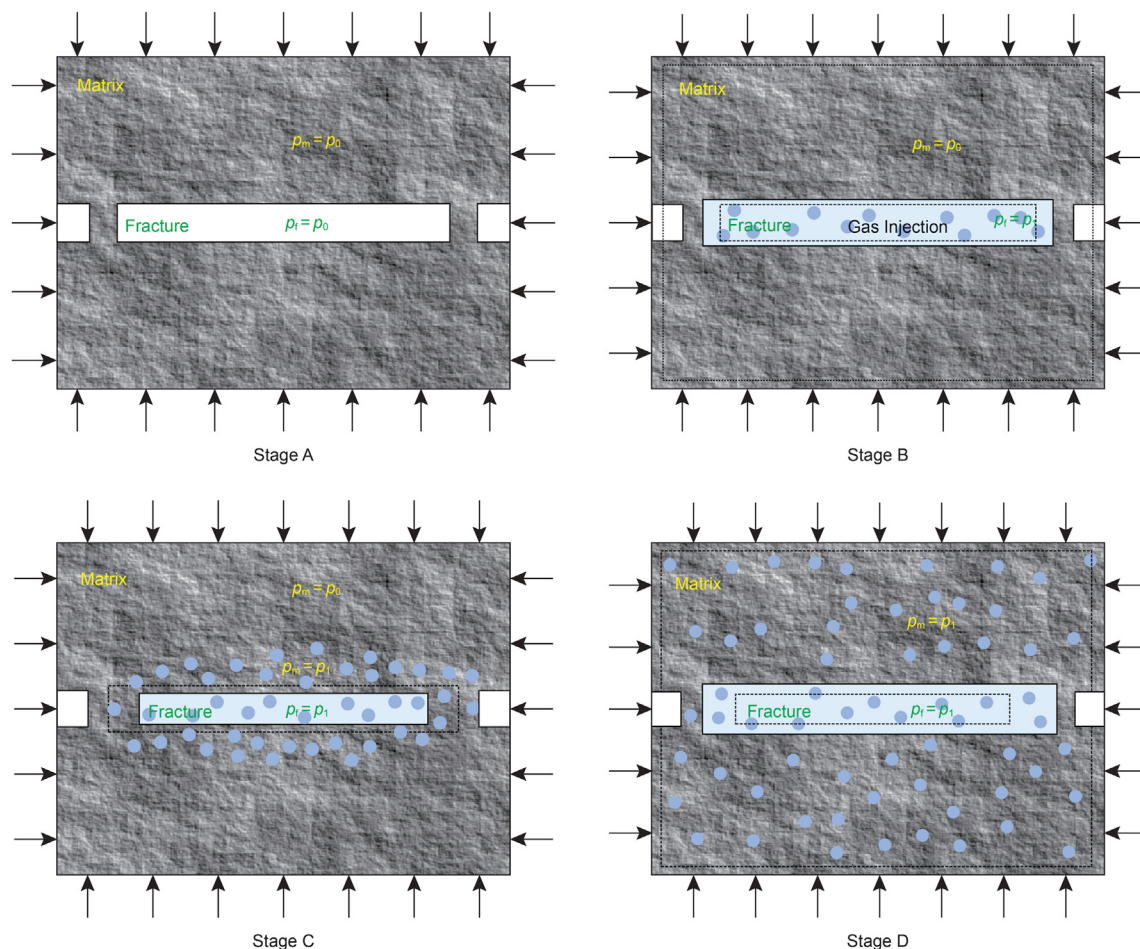
Fig. 1. The concept of local strain effect when gas injection.

With the rapid development of digital core technologies, especially the wide use of 3-D reconstruction of core samples through X-ray scan, accurate acquisition of pore distribution and fracture structure can be realized (Mostaghimi et al., 2017). Micro-CT imaging is based on the photon attenuation mechanism. It can achieve omni-directional scanning of the core sample. The X-ray detector receives the X-ray that penetrates the core and converts the X-ray signal into electrical signal. Then, the analog/digital converter translates the electrical signal into digital signal, which is finally stored in the computer (Liu et al., 2017). The photon flux interacts with rock minerals when the X-ray penetrates the rock, which induces photon energy attenuation. The attenuation amplitude can be calculated by Beer's equation (Barrett and Swindell, 1981):

$$I = I_0 e^{-\omega x}. \tag{1}$$

where I_0 is the original intensity of the X-ray, I is the intensity of the X-ray after penetrating the rock, ω is the attenuation coefficient, x is the X-ray transport distance within the core.

The coal sample was collected from Pingdingshan (Henan Province) at 310 m underground with a in-situ stress of 6.1 MPa. The sample, 50 mm in diameter and 100 mm long, belongs to high volatile bituminous coal. Coal maceral analyses show that the fractions of vitrinite, semi-vitrinite, liptinite, and inertinite are around 61.7%, 4.5%, 2.9%, and 30.9%, respectively. The apparatus we used is the Geoscan full-diameter core 3D CT system made by the Sanying Precision Instruments Ltd. with a resolution of 20 μm. To obtain the primary fracture geometry and reconstruct the fracture structure, post-scanning processes, such as noise filtration and image binarization processes, are conducted. The reconstructed fracture geometry is then imported in finite element software to simulate and analyze matrix and fracture pressure and stress distributions as well as matrix-fracture interactions during gas injection. Details of CT data processing are illustrated in Fig. 2.

(1) Noise filtration

The core images collected from the data normally contain a lot of noise, such as physical noise from the machine and salt-and-pepper noise. Median filtering is a commonly used filtering method which can mitigate the influence of noise and improve imaging quality. Therefore, median filtering is utilized to conduct noise filtration.

(2) Gray processing and image segmentation

The grayscale images are converted into binarized images through image binarization. Due to the distinct photon attenuation abilities of matrices and fractures, the binarized data of matrices and fractures are significantly different. Therefore, we select a threshold value to distinguish matrices from fractures. Here, the Otsu method is utilized to enhance the accuracy of image segmentation. Besides, coal contains a larger number of disconnected pores. We need to further remove the influence of isolated pores through filtering so that only primary interconnected fractures exist.
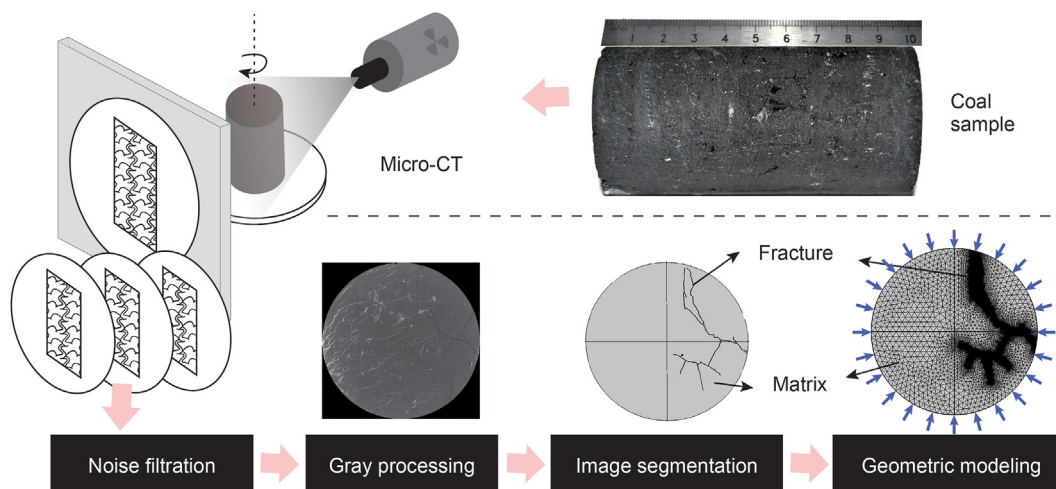
Fig. 2. Schematic diagram of CT data processing of the coal sample.

(3) Geometric modeling

Segmentation data of fractures are stored in the computer in the form of DXF files. These files can be directly imported in COMSOL Multiphysics software to reconstruct the sample and obtain the spatial distribution of fractures. The porous media without fractures are treated as matrices. Finally, the grid systems of fractures and matrices are established.

4. Mathematical models

To formulate the conceptual and geometric models, we first introduce the experimental procedure and corresponding boundary conditions. The sample is under a constant confining stress (pressure) condition. The gas is injected through the top of the sample and continuously adsorbs onto the sample. The upstream pressure is held constant, and the experiment ends when the adsorption equilibrium is reached. When gas is injected into the sample, the original equilibrium state between the matrix and fracture systems no longer exists. The coal sample first expands due to the effective stress reduction, enhancing the permeability. Then, the gas diffuses into matrices through fracture systems and adsorbs onto the fracture surfaces, which leads to matrix swelling and reduces fracture aperture. During this period, the permeability declines to some extent. To quantify how gas-sorption-induced deformation affects fracture space evolution, the governing equations for coal deformation and gas transport should be established to quantitatively describe the gas flow mechanisms within matrix and fracture systems after gas injection.

As for simulation, we idealize the physical process to reduce the complexity of the model and computational costs. The pore space structure and physical processes are shown in Fig. 3. The simulation model for fracture is discrete. Both fractures and matrices are treated as homogeneous and isotropic porous materials, while their mechanical and gas-transport properties are different. Fractures have higher permeability and the gas flow obeys Darcy's law. Matrix system involves pores and solid skeleton of coal and the methane is stored in the forms of adsorbed gas and free gas. The gas transport in matrix pores obeys Darcy's law, while the gas transport in the solid skeleton is realized through slippage effects and diffusion (Wei et al., 2016).

Other assumptions made to develop the model are listed below (Liu et al., 2020; Ma et al., 2019; Jiang et al., 2020):

(1) The coal seam is dry porous media and the influence of water on gas-solid coupling is ignored.
(2) The gas within coal is an ideal gas, and the viscosity is approximated as a constant under isothermal conditions.
(3) Gas transport is under an isothermal condition.
(4) The permeability of both matrix and fracture systems is isotropic.
(5) Fracture systems only contain free gas, while matrix gas includes adsorbed gas and free gas.

4.1. Governing equation for gas flow in the fracture system

In this study, the fracture system is treated as single-porosity media with homogeneous mechanical properties. The initial permeability of the sample is 10 μD, and the gas flow within fractures obeys Darcy's law. It is assumed that no source terms exist for mass balance equations of matrix and fracture. The gas pressure is equal between matrix-fracture interface. The mass balance equation is given by (Wei et al., 2019c)

$$\frac{d}{dt}\left(\phi_f p_f \frac{M}{RT}\right) - \nabla \cdot \left(\rho_g \frac{k_f}{\mu} \nabla p_f\right) = 0. \tag{2}$$

where ϕ_f is the porosity of the fracture system, p_f is the gas pressure in the fracture system, M is the molecular mass of gas, R is the universal gas constant, T is the absolute gas temperature, ρ_g is the gas density, μ is the viscosity coefficient and k_f is the permeability of the fracture system. Based on the previous study, the fracture permeability can be defined as a function of effective strain (Zhang et al., 2008). Both the strain and pore pressure in fractures control the fracture deformation. The strain is affected by external load and matrix strain. Thus, the fracture permeability is established as (Liu et al., 2011):

$$\frac{k_f}{k_{f0}} = \left(1 + \frac{\alpha}{\phi_{f0}}\left(\Delta\varepsilon_v + \frac{\Delta p_f}{K_f}\right)\right)^3. \tag{3}$$

where ϕ_{f0} and k_{f0} are the initial porosity and permeability of the fracture, α is the Biot coefficient, $\Delta\varepsilon_v$ is the increment of volumetric strain, and K_f is the bulk modulus of the fracture.
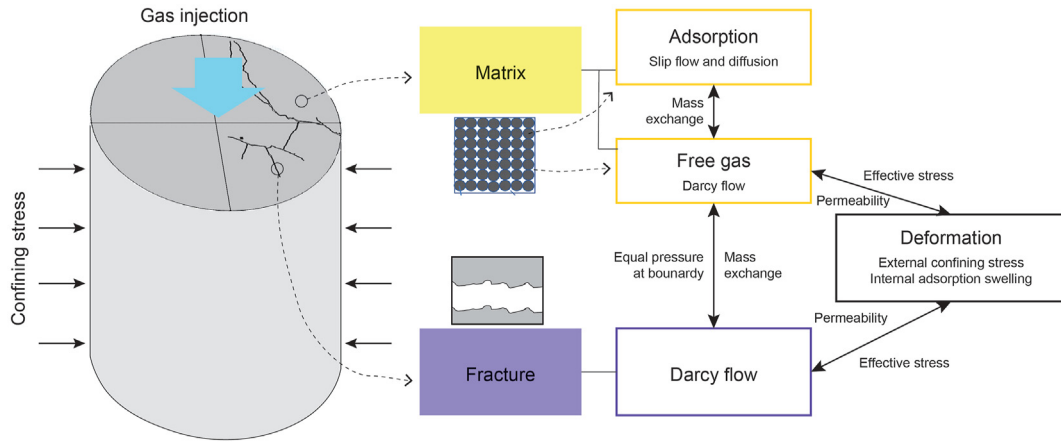
Fig. 3. Schematic diagram of gas-solid coupling in coal.

4.2. Governing equation for gas flow in the matrix

The matrix system consists of coal grains and small pores. Free-gas-phase methane flows within micropores, and the rest of methane is stored in coal grains in the form of an adsorbed phase. Due to the existence of gas slippage and diffusion in nanopores, the apparent permeability concept is usually employed to represent the permeability of the sample. Therefore, the mass balance equation for matrix gas transport can be written as (Wei et al., 2019c):

$$\frac{\mathrm{d}}{\mathrm{d}t}\left(\phi_m p_m \frac{M}{RT} + (1-\phi_m)\rho_{ga}\rho_m \frac{V_L p_m}{P_L + p_m}\right) - \nabla\cdot\left(\rho_g \frac{k_m}{\mu}\nabla p_m\right) = 0 \tag{4}$$

where ϕ_m is the porosity of the matrix system, p_m is the gas pressure in the matrix, ρ_{ga} is gas density at atmospheric pressure, ρ_m is the coal matrix density, V_L is the Langmuir volume constant, and P_L is the Langmuir pressure constant, k_m is the permeability of the matrix. The permeability is affected by both flow regimes and pore deformation. The flow regime is determined by the Knudsen number (Kn), while pore deformation is dominated by external loads and internal sorption-induced deformation. Consequently, the matrix permeability is expressed as (Florence et al., 2007; Wei et al. 2016, 2018):

$$k_m = k_{m\infty} f(Kn) \tag{5}$$

where $k_{m\infty}$ is the intrinsic permeability. The variation of intrinsic permeability depends on pore deformation. The f-function ($f(Kn)$) denotes flow regime correction and is a function of Kn. Because the intrinsic permeability is essentially dependent on external loads and internal sorption-induced deformation, it can be written as a function of the effective strain:

$$\frac{k_{m\infty}}{k_{m0}} = \left(1 + \frac{\alpha}{\phi_m}\left(\Delta\varepsilon_v + \frac{\Delta p_m}{K_m} - \Delta\varepsilon_s\right)\right)^3 \tag{6}$$

where k_{m0} is the initial matrix permeability, $\Delta\varepsilon_v$ is the external-load-induced volumetric strain change, K_m is the modulus of the solid matrix skeleton, and $\Delta\varepsilon_s$ is the change in sorption-induced matrix strain. Micro-scale flow through coal matrices involves various distinct transport mechanisms. Flow regimes can be classified based on the Knudsen number. For Knudsen numbers less than 0.01, the use of the ideal gas constant in Darcy's law and the assumption of continuum flow remain valid. When the Knudsen number is within the range of 0.01−0.1, the flow lies in the slip regime. Both slip and diffusion flow occur in the transition flow regime, where the Knudsen numbers are greater. Gas diffusion is commonly considered to take palace in coal matrices during the sorption and desorption procedures. The correction for continuum flow is required in coal matrices. The apparent permeability is a function of pressure in the slip, transitional, and Knudsen flow regimes due to molecular interaction with the porous medium. It is written as (Civan, 2010):

$$f(Kn) = (1+\beta Kn)\left(1 + \frac{4Kn}{1+Kn}\right) \tag{7}$$

The Knudsen numbers are defined as the ratio of the gas mean free path λ to the characteristic length $2r$, and is given by:

$$Kn = \frac{\gamma}{2r} \tag{8}$$

$$\gamma = \frac{k_B T}{\sqrt{2}\pi d_g^2 p_m} \tag{9}$$

$$\beta = \frac{128}{15\pi^2}\tan^{-1}\left(4Kn^{0.4}\right) \tag{10}$$

where k_B is the Boltzmann constant; d_g is the effective molecular diameter; β-parameter is a function of Kn. Substituting Eqs. (6) and (7) into Eq. (5), the multi-scale permeability model for the coal matrix system is defined as (Wei et al., 2016):

$$k_m = k_{m0}\left(1 + \frac{\alpha}{\phi_{m0}}\left(\Delta\varepsilon_v + \frac{\Delta p_m}{K_m} - \Delta\varepsilon_s\right)\right)^3$$
$$(1+\beta Kn)\left(1 + \frac{4Kn}{1+Kn}\right) \tag{11}$$

This model fully covers the influence of effective stress at the macroscopic scale and flow regimes at the microscopic scale on the change of matrix permeability. The adsorption-induced swelling and gas pressure are the dominant factors that control matrix permeability during gas injection.

4.3. Governing equation for rock deformation

For coal matrix and fracture deformation, the strain tensor is generally written as displacement components, as shown below (Zhang et al., 2008)

$$\varepsilon_{ij} = \left(u_{i,j} + u_{j,i}\right) \qquad (12)$$

where ε_{ij} is the strain tensor, u is the displacement component, and i and j represent the coordinate. By ignoring the inertia force, the force equilibrium equation is given by (Zhang et al., 2008)

$$\sigma_{ij,i} + f_j = 0 \qquad (13)$$

where σ_{ij} is the total stress tensor component, and f_j is the body force component. According to the theory of continuum mechanics, the combination of the equilibrium equation and the constitutive equations for the homogeneous, isotropic, and elastic medium derives the Navier-type equation (Wu et al., 2010),

$$Gu_{i,kk} + \frac{G}{1-2\nu}u_{k,ik} - \alpha p_i - K\varepsilon_L \frac{P_L}{(p_i + P_L)^2}p_i + f_i = 0 \qquad (14)$$

where u_i is the component of displacement in the i-direction, G is the shear modulus, ν is the Poisson's ratio, f_i is the component of body force in the i-direction, and ϵ_L is the Langmuir volumetric strain constant in matrix. Note that ϵ_L is zero in the fracture. The deformation induced by adsorption swelling and pore pressure are considered in this equation. The interaction between matrix and fracture is included in the term of volumetric strain. The coupling relationship between gas flow and deformation is established based on the diffusion coefficient that is affected by deformation. The gas pressure distribution also has a large impact on the effective stress according to the effective stress law.

5. Numerical models

In this paper, COMSOL Multiphysics is utilized to conduct numerical simulation. It is a finite-element-method-based software that performs multiphysics modeling through solving the partial differential equation (single-physics) or partial differential equation groups (Multiphysics). The calculation basically follows the following steps:

(1) Geometric model import

The fracture structure is extracted from gray level quantization. Before exporting the fracture geometry, the smoothing of fracture structure is performed to facilitate gridding and calculation. The extracted fracture structure is saved as a DXF file and imported into COMSOL through the import command of Geometry. Finally, the matrix and fracture domains are generated in COMSOL through 'Difference' and 'Union' commands. The resulting geometry is shown in Fig. 2.

(2) Physics module selection

Three physics modules (Eqs. (2), (4) and (14)) are built in COMSOL Multiphysics, including Darcy's law, Solid Mechanics, and Coefficient Form PDE. Therefore, the equations are solved thorough fully coupled processes. Major input parameters for numerical simulation are given in Table 1. Some parameters which are not available during our laboratory tests are collected from a recently published paper (Wei et al., 2019a) to ensure their rationality.

(3) Boundary conditions

The boundaries conditions are in accordance with the permeability testing conditions and the experimental procedure. Details are provided below: (a) Methane diffusion in matrices and methane

Table 1
Parameters for simulation.

Parameters	Values
Coal density, kg/m^3	1400
Gas density under the standard condition, kg/m^3	0.71
Bulk modulus of the matrix, GPa	10
Bulk modulus of the fracture, GPa	0.5
CO_2 viscosity, Pa s	1.84×10^{-5}
Langmuir volume constant, m^3/kg	0.015
Langmuir pressure, MPa	6.109
Fracture porosity, m^2	0.027
Fracture permeability	1×10^{-17}
Matrix diffusivity, m/s	1×10^{-9}
Matrix permeability, m^2	1×10^{-20}

flow in fractures: the sample has no-flow boundaries where the methane flux is zero. The gas inlet is located at the center of the fracture within the coal sample. Gas injection is performed under a fixed pressure level (3 MPa). (b) Coal deformation field: A constant confining pressure condition is applied to the sample. The confining pressure is 6 MPa. (c) Initial condition: Matrix and fracture systems are under a pressure-equilibrium condition. They are both in a vacuum environment.

(4) Mesh generation

The selection of mesh types determines the accuracy of calculation results. In this study, grids are defined as triangular elements, and the local grid refinement method is utilized as shown in Fig. 2. There are in total 98547 vertices and 196902 units.

(5) Simulation

After completing the above steps, one needs to select Time Dependent Study in COMSOL and choose an appropriate time step. When conducting sensitivity analyses to find the dominant parameters for permeability evolution, we can also use the Parametric Sweep command to change the parameter we investigated automatically.

6. Results and discussion

6.1. Pore-pressure-propagation-induced deformation evolution

When CO_2 is injected into the sample, the gas gradually moves within matrix and fracture systems due to pressure drive and
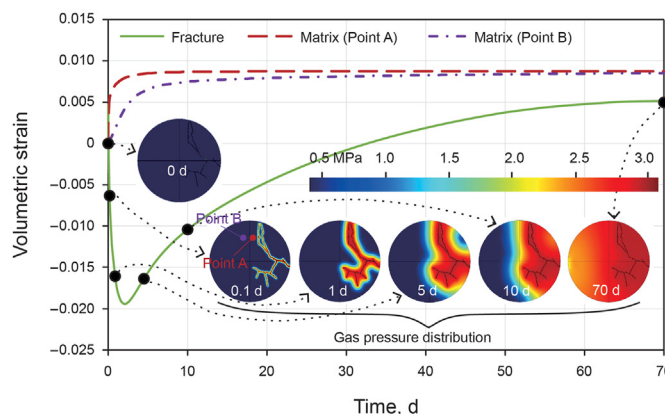

Fig. 4. Evolution of volumetric strains of selected points for fracture and matrix systems during CO_2 injection.

adsorbs onto the rock. Fig. 4 demonstrates the pressure distribution during gas injection at different times (0, 0.1, 1, 5, 10, and 70 d, respectively). The fracture strain curve is generated from the data of a point within the fracture, while matrix strain data are collected from matrix points A and B, which are 1 mm and 5 mm away from the fracture point as shown in Fig. 4. Before gas injection, the sample is under an equilibrium state without matrix-fracture interaction. After 0.1 d, the maximum fracture strain increment is 0.005 because the fracture permeability is relatively high, and the gas enters the fracture rapidly, resulting in an effective-stress-reduction-induced volume increment. The fracture pressure equilibrium (homogeneous distribution) is reached within a short period. Meanwhile, the amount of gas that diffuses into the matrix is relatively small. This results in a matrix-fracture pressure difference. With gas injection continues, more gas enters the matrix through matrix-fracture interfaces. The combined effects of gas-sorption-induced swelling and the matrix gas pressure increase cause the localized matrix swelling near fracture surfaces. With the pressure propagation within matrices, it can be seen that the matrix swelling area expands. Matrix swelling first occurs at point A, and this is followed by point B. In this situation, fractures become narrower due to the adjacent matrix swelling induced compaction. Later, matrices near fractures almost achieve an equilibrium state, and fracture compaction and localized swelling effects become smaller. Accordingly, fracture volumetric strains start to increase. With gas diffusion into matrices goes on, the swelling area continuously increases until the pressure wave propagation covers the whole matrix system. At this stage, a new matrix-fracture equilibrium state is reached. Results show that the fracture volume decreases when matrices swell and generate fracture compaction due to the non-uniform fracture distribution. These conclusions are consistent with results obtained in previous studies (Wu et al., 2010; Wei et al., 2019a; Liu et al., 2020).

6.2. Permeability evolution under constant confining pressure conditions

Experimental measurements of the coal sample have been conducted (Wei et al., 2019b). The coal sample was confined under a constant boundary stress. Then the upstream boundary of the sample was exposed to CO_2 at a fixed gas pressure. The CO_2 was adsorbed constantly for a long-term stage. Coal permeability was measured continuously throughout the entire period of the experiment from the initial to final equilibrium. The measured permeability changes significantly as shown in Fig. 5.

Fig. 5 also shows simulated permeability evolution during absorbable gas (CO_2) and non-adsorbable gas (He) injection under
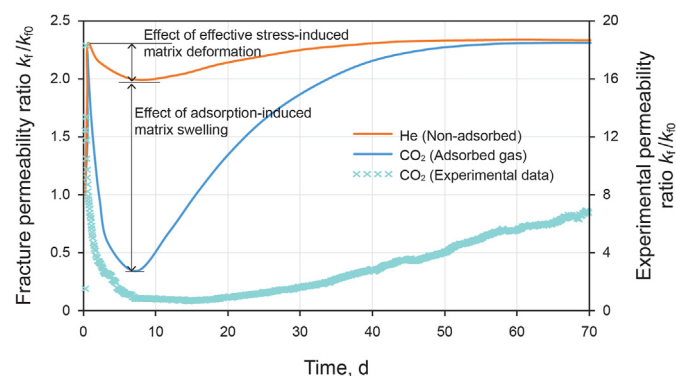

Fig. 5. Evolution of permeability for adsorbing gas (CO_2) and non-adsorbing gas (He) injection under conditions of a constant confining stress.

constant confining pressure conditions. It is obvious that the trend of simulation result for absorbable gas is consistent with that of experimental data. Note that the variation of simulation results is smaller than the experimental data. It is because of the simulation model is a 2D cross section of experimental coal core. And the selected section can represent the evolution of fracture permeability. The variation tendency of two curves are basically consistent. However, the variable quantity is depended on the properties of fracture and matrix. Permeability curves of the two types of gases both experienced four stages: (1) Permeability enhancement stage: fracture permeability is relatively high, which leads to a rapid pressure increase within fractures. The fracture pressure growth reduces the effective stress and causes permeability enhancement. (2) Permeability decline stage: during this period, gas adsorbs onto matrix surfaces and diffuses into the matrix. Localized matrix swelling merely occurs near the fracture and reduces fracture permeability, which also refers to the local swelling stage. (3) Permeability rebound stage: with more gas enters the matrix, fracture permeability starts to rebound and is controlled by the external boundary conditions. This period is treated as a global-behavior controlled stage. (4) Permeability stable stage: after a long-time gas injection procedure, gas pressure within the matrix gradually reaches an equilibrium state, and the permeability consequently turns stable. Compared with the permeability measurement data of non-absorbable gas, there is a more obvious permeability decline period for absorbable gas. This is because non-absorbable gas injection only reduces the effective stress of the matrix system and increases the matrix volume. However, absorbable gas injection provides additional sorption-induced matrix swelling, resulting in the total matrix volume increment far larger than that during non-absorbable gas injection (Wei et al., 2019b). This is the reason for a broader range of fracture permeability change during CO_2 injection. The permeability drop for the absorbable gas is six times that of the non-absorbable gas, which indicates that sorption-induced matrix deformation effects on permeability evolution should not be ignored when investigating absorbable gas's influence on permeability.

The inconsistency of measured permeability and conventional theoretical prediction in stage 3 is caused by the local swelling of the matrix (Liu et al., 2011). When the matrix swelling deformation is localized in the vicinity of the fracture wall, the swelling area reduces the fracture opening. At this stage, the coal permeability is controlled primarily by the internal structure. After the gas flow through the matrix, swelling deformation expand to the whole sample. In this stage, the swelling deformation is nearly uniform. The coal permeability is unchanged with the pressure equilibrated in matrix.

6.3. Sensitivity analyses under constant confining pressure conditions

From the above results, it is clear that sorption-induced matrix deformation affects the fracture volume. Therefore, sorption-induced matrix deformation related parameters, such as injection pressure, matrix swelling strains, and matrix permeability, are closely related to permeability evolution. In order to compare the effects of sorption-induced strains, pore pressure, matrix permeability on fracture permeability, sensitivity analyses are performed based on the cases shown in Table 2.

As shown in Fig. 6, under different injection pressures, the lowest permeability ratio and the final equilibrium permeability ratio both increase with the increment of injection pressure. The higher the injection pressure is, the larger the fracture aperture increases at initial times would be, and the higher the final equilibrium permeability increment would be. The influence of

Table 2
Simulation scenarios.

	Injection pressure p_i, MPa	Langmuir volumetric strain constant ε_L	Initial permeability of matrix k_{m0}, nD	Results
Case 1	3	0.01 (CO_2); 0 (Helium)	10	Fig. 5
Case 2	2, 3, 4, 5	0.01	10	Fig. 6
Case 3	3	0.001, 0.005, 0.01, 0.02	10	Fig. 7
Case 4	3	0.01	1, 10, 100, 1000	Fig. 8
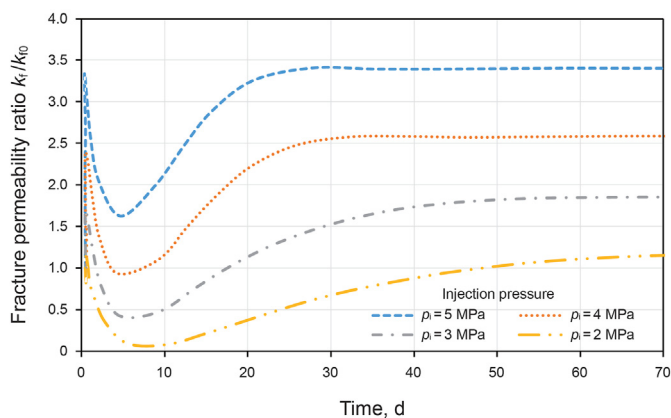
Fig. 6. Evolution of permeability for adsorbing gas (CO_2) under different injection pressures at a constant confining stress.

injection pressure on the permeability ratio decline is relatively small. The permeability ratio decline ranges under the four injection cases are almost identical. When the injection pressure is low, the pressure gradient drives the gas flow slower, resulting in the weakening of matrix swelling effects on the fracture aperture change. It is shown that the permeability rebound period slows down when the injection pressure is 2 MPa.

Fig. 7 presents fracture permeability evolution with different Langmuir strain constants of matrix. With increases of the Langmuir strain constant, the permeability reduction becomes stronger, while the final equilibrium permeability values are almost the same. This indicates that the larger the matrix deformation is, the heavier its influence on fracture volume compaction will be. However, when the matrix pressure reaches equilibrium and the localized matrix swelling becomes global swelling, the sample regains the lost fracture volume. The Langmuir strain constant only affects the intermediate stage of permeability evolution with no influence on the final equilibrium permeability.
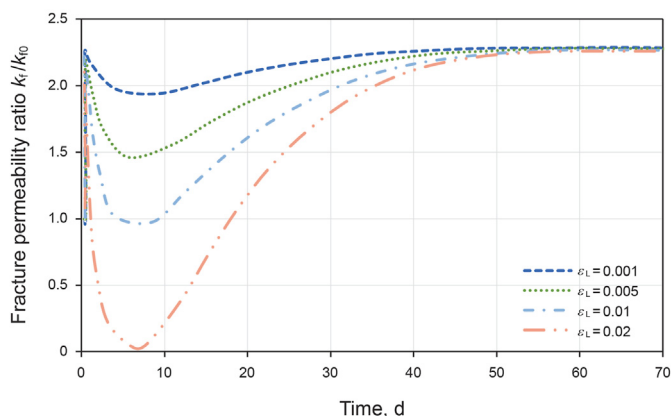
Rapid gas transport occurs in fractures, while the gas diffuses slowly within matrices. Fig. 8 shows the permeability evolution under different initial matrix permeability values. Results reveal that the matrix initial permeability not only affects the magnitude of the fracture permeability drop but also influences the duration of the permeability rebound. With an increase in the initial matrix permeability, the time required to achieve matrix pressure equilibrium is shorter, and the magnitude of the permeability decline is smaller. With a higher initial permeability value, the matrix pore pressure achieves an equilibrium state rapidly, which mainly induces global swelling. This mitigates the fracture compaction effects caused by localized matrix swelling, and the duration of the permeability reduction is relatively short. When the initial permeability of the matrix is extremely low, the localized matrix swelling near fracture surfaces occupies a long time during which the fracture system is in a compacted state. Therefore, the magnitude of the fracture permeability reduction is large, and this reduction period lasts for a long time. Note that the matrix initial permeability only changes the equilibrium time, and the final equilibrium fracture permeability of different cases is identical.

7. Conclusions

This study investigates the influences of sorption-induced coal swelling on the permeability of heterogeneously distributed fractures. The micro-CT system is used to obtain the real fracture distribution, and the coal geometric model is built based on the actual fracture geometry. Theoretical models for gas flow and mechanical responses of matrix and fracture systems are derived to simulate and analyze the pressure propagation within matrices and fractures and matrix-fracture deformation during gas injection. Fracture permeability evolutions during the process of gas adsorption are obtained. The following major conclusions are drawn:

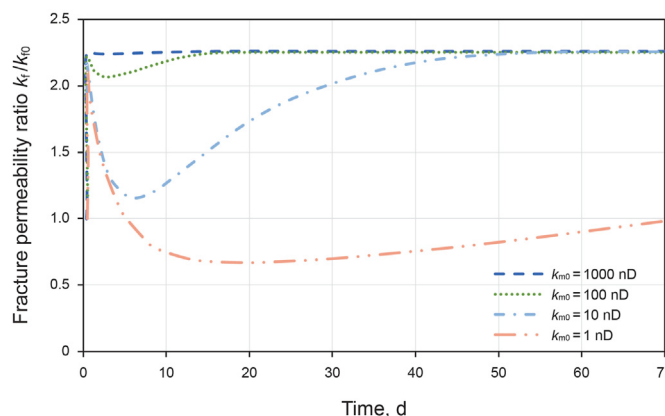(1) A simple reconstruction method for fully-coupled gas-flow and rock-deformation process simulation within actual

Fig. 7. Evolution of permeability for adsorbing gas (CO_2) under different Langmuir matrix strain constants at a constant confining stress.

Fig. 8. Evolution of permeability for adsorbing gas (CO_2) under different initial matrix permeability values at a constant confining stress.

fractured coal samples is established. This method involves fracture characterization, fracture geometry and extraction, and explicit geometric model construction based on actual fracture distribution. The mass balance equation for the fracture system is derived with consideration of the influence of external loads and effective stress on permeability. Based on gas adsorption, diffusion, viscous flow, and slippage, the matrix mass balance equation is figured out, accounting for the effects of external loads, sorption-induced swelling, and effective stress on permeability.

(2) The simulation replicates matrix-fracture interactions caused by sorption-induced matrix swelling. Gas injection initially reduces the effective stress of the fracture system, which enhances fracture permeability. Later on, the matrix gas pressure rises, which diminishes effective-stress-induced deformation and generates sorption-induced swelling deformation. This results in the fracture volume compaction and a consequential fracture permeability reduction. When the whole porous system approaches the equilibrium state, the global swelling of the sample occurs, and the fracture permeability rebounds.

(3) Sensitivity analyses quantify the impacts of injection pressure, Langmuir strain constant, and initial matrix permeability on fracture permeability evolution. A higher injection pressure level generates a larger permeability increment and a lower fracture permeability drop during the localized matrix swelling period. The larger the Langmuir strain constant is, the heavier the fracture permeability drop will be during localized swelling. The matrix initial permeability controls the magnitude of the permeability drop and the duration of permeability rebound. The lower the initial matrix permeability is, the larger the fracture permeability drop caused by localized swelling will be, and the longer the permeability rebound period will last.

Availability of data and material

Not applicable.

Declaration of competing interest

The authors declare that they have no conflict of interest.

Acknowledgments

Code availability

Not applicable.

Authors' contributions

The manuscript was written through contributions of all authors. All authors have given approval to the final version of the manuscript.

References

Al-Kharusi, A.S., Blunt, M.J., 2007. Network extraction from sandstone and carbonate pore space images. J. Petrol. Sci. Eng. 56 (4), 219–231. https://doi.org/10.1016/j.petrol.2006.09.003.

Barrett, H.H., Swindell, W., 1981. Radiological Imaging: the Theory of Imaging Formation. Detection and Processing. Academic Press, New York. https://doi.org/10.1063/1.2915593.

Brochard, L., Vandamme, M., Pellenq, R.J.M., 2012. Poromechanics of microporous media. J. Mech. Phys. Solid. 60, 606–622. https://doi.org/10.1016/j.jmps.2012.01.001.

Civan, F., 2010. Effective correlation of apparent gas permeability in tight porous media. Transport Porous Media 82 (2), 375–384. https://doi.org/10.1007/s11242-009-9432-z.

Connell, L.D., Detournay, C., 2009. Coupled flow and geomechanical processes during enhanced coal seam methane recovery through CO_2 sequestration. Int. J. Coal Geol. 77, 222–233. https://doi.org/10.1016/j.coal.2008.09.013.

Connell, L.D., Lu, M., Pan, Z., 2010. An analytical coal permeability model for tri-axial strain and stress conditions. Int. J. Coal Geol. 84 (2), 103–114. https://doi.org/10.1016/j.coal.2010.08.011.

Cui, X., Bustin, R.M., Chikatamarla, L., 2007. Adsorption-induced coal swelling and stress: implications for methane production and acid gas sequestration into coal seams. J. Geophys. Res. 112, B10202 https://doi.org/10.1029/2004JB003482.

Fan, D., Ettehadtavakkol, A., 2017. Semi-analytical modeling of shale gas flow through fractal induced fracture networks with microseismic data. Fuel 193, 444–459. https://doi.org/10.1016/j.fuel.2016.12.059.

Florence, F.A., Rushing, J.A., Newsham, K.E., Blasingame, T.A., 2007. Improved permeability prediction relations for low permeability sands. In: SPE Rocky Mountain Oil and Gas Technology Symposium, Denver, Colorado, USA, 16-18 April, 2007. Society of Petroleum Engineers. https://doi.org/10.2523/107954-MS.

He, S., Jiang, Y., Conrad, J.C., Qin, G., 2015. Molecular simulation of natural gas transport and storage in shale rocks with heterogeneous nano-pore structures. J. Petrol. Sci. Eng. 133, 401–409. https://doi.org/10.1016/j.petrol.2015.06.029.

Jiang, C.Z., Zhao, Z., Zhang, X.W., et al., 2020. Controlling effects of differential swelling index on evolution of coal permeability. J. Rock Mechan. Geotechn. Eng. 12 (3), 461–472. https://doi.org/10.1016/j.jrmge.2020.02.001.

Liu, J.S., Chen, Z.W., Elsworth, D., Qu, H.Y., Chen, D., 2011. Interactions of multiple processes during CBM extraction: a critical review. Int. J. Coal Geol. 87, 175–189. https://doi.org/10.1016/j.coal.2011.06.004.

Liu, Q.Q., Cheng, Y.P., Ren, T., Jing, H.W., Tu, Q.Y., Dong, J., 2016. Experimental observations of matrix swelling area propagation on permeability evolution using natural and reconstituted samples. J. Nat. Gas Sci. Eng. 34, 680–688. https://doi.org/10.1016/j.jngse.2016.07.035.

Liu, S., Sang, S., Wang, G., Ma, J., Wang, X., Wang, W., Du, Y., Wang, T., 2017. FIB-SEM and X-ray CT characterization of interconnected pores in high-rank coal formed from regional metamorphism. J. Petrol. Sci. Eng. 148, 21–31. https://doi.org/10.1016/j.petrol.2016.10.006.

Liu, X.X., Sheng, J., Ma, C., et al., 2020. Complete coal permeability models from initial to ultimate equilibrium. Fuel 271, 117612. https://doi.org/10.1016/j.fuel.2020.117612. Jc.

Ma, X., Li, X., Zhang, S.W., et al., 2019. Impact of local effects on the evolution of unconventional rock permeability. Energies 12 (3), 478. https://doi.org/10.3390/en12030478.

Mostaghimi, P., Armstrong, R.T., Gerami, A., et al., 2017. Cleat-scale characterization of coal: an overview. J. Nat. Gas Sci. Eng. 39, 143–160. https://doi.org/10.1016/j.jngse.2017.01.025.

Nikoosokhan, S., Vandamme, M., Dangla, P., 2012. A poromechanical model for coal seams injected with carbon dioxide: from an isotherm of adsorption to a swelling of the reservoir. Oil Gas Sci. Technol. - Rev. IFP Energies Nouvelles 67 (5), 777–786. https://doi.org/10.2516/ogst/201204.

Nikoosokhan, S., Vandamme, M., Dangla, P., 2014. A poromechanical model for coal seams saturated with binary mixtures of CH_4 and CO_2. J. Mech. Phys. Solid. 71, 97–111. https://doi.org/10.1016/j.jmps.2014.07.002.

Palmer, I., Mansoori, J., 1996. How permeability depends on stress and pore pressure in coalbeds: a new model. SPE Reservoir Eval. Eng. 1 (6), 539–544. https://doi.org/10.2118/52607-PA.

Robertson, E.P., Christiansen, R.L., 2008. A permeability model for coal and other fractured sorptive-elastic media. SPE J. 13, 314–324. https://doi.org/10.2118/104380-PA.

Seidle, J., Huitt, L., 1995. Experimental measurement of coal matrix shrinkage due to gas desorption and implications for cleat permeability increases. International Meeting on Petroleum Engineering, Beijing, China, November. Society of Petroleum Engineers. https://doi.org/10.2523/30010-MS.

Shi, J.Q., Durucan, S., 2005. A model for changes in coalbed permeability during primary and enhanced methane recovery. SPE Reservoir Eval. Eng. 8 (4), 291–299. https://doi.org/10.2118/87230-PA.

Shi, R., Liu, J.S., Wei, M.Y., Elsworth, D., Wang, X.M., 2018. Mechanistic analysis of coal permeability evolution data under stress-controlled conditions. Int. J. Rock Mech. Min. Sci. 110, 36–47. https://doi.org/10.1016/j.ijrmms.2018.07.003.

Vandamme, M., Brochard, L., Lecampion, B., Coussy, O., 2010. Adsorption and strain: the CO_2-induced swelling of coal. J. Mech. Phys. Solid. 58, 1489–1505. https://doi.org/10.1016/j.jmps.2010.07.014.

Wang, K., Zang, J., Wang, G., et al., 2014. Anisotropic permeability evolution of coal

with effective stress variation and gas sorption: model development and analysis. Int. J. Coal Geol. 130, 53—65. https://doi.org/10.1016/j.coal.2014.05.006.

Wei, M.Y., Liu, J.S., Feng, X.T., Wang, C.G., Zhou, F.B., 2016. Evolution of shale apparent permeability from stress-controlled to displacement-controlled conditions. J. Nat. Gas Sci. Eng. 34, 1453—1460. https://doi.org/10.1016/j.jngse.2016.07.012.

Wei, M.Y., Liu, J.S., Elsworth, D., Wang, E.Y., 2018. Triple porosity modelling for the simulation of multi-scale flow mechanisms in shale reservoirs. Geofluids, 6948726. https://doi.org/10.1016/j.jngse.2016.07.012.

Wei, M.Y., Liu, J.S., Elsworth, D., 2019a. Influence of Gas adsorption induced non-uniform deformation on the evolution of coal permeability. Int. J. Rock Mech. Min. Sci. 114, 71—78. https://doi.org/10.1016/j.ijrmms.2018.12.021.

Wei, M.Y., Liu, J.S., Shi, R., et al., 2019b. Long-term evolution of coal permeability under effective stresses gap between matrix and fracture during CO_2 injection.

Transport Porous Media 130 (6), 1—15. https://doi.org/10.1007/s11242-019-01350-7.

Wei, M.Y., Liu, Y.K., Liu, J.S., Elsworth, D., Zhou, F.B., 2019c. Micro-scale investigation on coupling of gas diffusion and mechanical deformation of shale. J. Petrol. Sci. Eng. 175, 961—970. https://doi.org/10.1016/j.petrol.2019.01.039.

Wu, Y., Derek, E., Chen, Z., Connell, L.D., Pan, Z., 2010. Dual poroelastic response of a coal seam to CO_2 injection. Int. J. Greenh. Gas Control 4 (4), 668—678. https://doi.org/10.1016/j.ijggc.2010.02.004.

Wu, W., Zoback, M., Kohli, A., 2017. The impacts of effective stress and CO_2 sorption on the matrix permeability of shale reservoir rocks. Fuel 203, 179—186. https://doi.org/10.1016/j.fuel.2017.04.103.

Zhang, H.B., Liu, J.S., Elsworth, D., 2008. How sorption-induced matrix deformation affects gas flow in coal seams: a new FE model. Int. J. Rock Mech. Min. Sci. 45, 1226—1236. https://doi.org/10.1016/j.ijrmms.2007.11.007.